

# Engineered Cementitious Composites with High-Volume Fly Ash

by Shuxin Wang and Victor C. Li

*Engineered cementitious composites (ECCs) are a breed of high-performance fiber-reinforced cementitious composites (HPFRCC) with significant strain-hardening behavior under tension. As ECCs impart ductility and durability to the structure, the high cement usage in the mixture causes environmental and economical impacts. In this paper, the mechanical performance of ECCs incorporating high volume fly ash and bottom ash is reported. Emphasis is placed on the influence of fly ash content on the key micromechanics properties relevant to composite ductility. It is revealed that a high volume fraction of fly ash tends to reduce the polyvinyl alcohol (PVA) fiber/matrix interface bond and matrix toughness in favor of attaining high tensile strain capacity. The limit of cement substitution with ash is constrained by compressive strength development.*

**Keywords:** cementitious; fiber; fly ash.

## INTRODUCTION

Engineered cementitious composites (ECCs) are a unique class of the new generation high-performance fiber-reinforced cementitious composites (HPFRCC) featuring high ductility and medium fiber content. Tensile strain capacity at a range of 3 to 5% has been demonstrated in ECC materials using polyethylene fibers and polyvinyl alcohol (PVA) fibers with fiber volume fraction no greater than 2%.<sup>1,2</sup> The large strain is contributed by sequential development of multiple cracks, instead of continuous increase of the crack opening. The associated high fracture toughness and controlled crack width (typically below 100  $\mu\text{m}$  [0.004 in.]) make ECCs an ideal material to improve serviceability and durability of infrastructures. In recent years, the field application of ECCs has increased. The material has been successfully applied to dam repair, bridge deck overlays, coupling beams in high-rise buildings, and other structural elements and systems.<sup>3</sup>

Material engineering of ECCs is constructed on the paradigm of the relationships between material microstructures, processing, material properties, and performance, where micromechanics is highlighted as the unifying link between composite mechanical performance and material microstructure properties.<sup>4</sup> The established micromechanics models guide the tailoring of composite constituents including fiber, matrix, and interface for overall performance, and elevate the material design from trial-and-error empirical testing to systematic, holistic, engineered combination of individual constituents. The microstructure to composite performance linkage can be further extended to the structural performance level and integrate the material design into performance-based design concept for structures.<sup>5</sup> In that sense, ECCs embody a material design approach in addition to being an advanced material and provide an additional degree of freedom in structural performance design.

Compared with conventional concrete, ECC materials contain considerably higher cement content, typically two to

**Table 1—Mixture proportions of concrete and ECC materials**

Material	Cement, kg/m <sup>3</sup> (lb/yd <sup>3</sup> )	Aggregates, kg/m <sup>3</sup> (lb/yd <sup>3</sup> )	Water, kg/m <sup>3</sup> (lb/yd <sup>3</sup> )	HPMC,* kg/m <sup>3</sup> (lb/yd <sup>3</sup> )	HRWRA, kg/m <sup>3</sup> (lb/yd <sup>3</sup> )	Fiber, kg/m <sup>3</sup> (lb/yd <sup>3</sup> )
Concrete	390 (657)	1717 (2894)	166 (280)	—	—	—
PE-ECC	1205 (2031)	603 (1016)	314 (529)	0.60 (1.0)	12 (20)	17 (29)
PVA-ECC R0	832 (1402)	832 (1402)	366 (617)	1.26 (2.1)	17 (29)	26 (44)

\*Hydroxypropyl methylcellulose—viscosity agent.

three times higher. Table 1 shows the mixture proportions of typical (high modulus) polyethylene ECC (PE-ECC)<sup>1</sup> and PVA-ECC,<sup>2</sup> along with conventional structural concrete. The high cement content in ECCs is a consequence of rheology control for easy fiber dispersion and, more essentially, matrix toughness control for strain-hardening behavior. To achieve strain hardening, matrix fracture toughness has to be limited such that multiple cracking could occur before reaching maximum fiber bridging stress. Large aggregates are hence eliminated in the mixture, resulting in a higher cement content compared with normal concrete. In fact, ECC materials use cement paste or mortar with fine sand as a matrix, and typically have cement content at 830 to 1200 kg/m<sup>3</sup> (1400 to 2023 lb/yd<sup>3</sup>). High cement usage results in undesired high hydration heat as well as high material cost. In addition, such matrixes apparently compromise sustainability performance of the material, as cement production is responsible for 3% of global greenhouse gas emissions generated by human activities,<sup>6</sup> and significant levels of nitrogen oxides, particulate matter, and other pollutants. High cement content is also commonly found in many other types of HPFRCC materials, such as slurry-infiltrated fiber concrete<sup>7</sup> and fiber reinforced reactive powder concrete composite.<sup>8</sup>

One natural approach to address these issues is to substitute cement with industrial by-products. Coal combustion products (CCPs) are of particular interest due to their abundant availability. For example, the electrical utility industry in the US generated approximately 121 million tons (267 million klb) of CCPs in 2003, including 70.2 million tons (155 million klb) of fly ash and 18.1 million tons (40 million klb) of bottom ash. Only 46 million tons (101 million klb) were recycled and

ACI Materials Journal, V. 104, No. 3, May-June 2007.

MS No. M-2005-170 received August 8, 2005, and reviewed under Institute publication policies. Copyright © 2007, American Concrete Institute. All rights reserved, including the making of copies unless permission is obtained from the copyright proprietors. Pertinent discussion including authors' closure, if any, will be published in the March-April 2008 ACI Materials Journal if the discussion is received by December 1, 2007.

**Shuxin Wang** is Manager, MSeals Co. Ltd., Ningbo, China. He received his PhD from the Department of Civil and Environmental Engineering at the University of Michigan, Ann Arbor, Mich. His research interests include the development of high-performance fiber-reinforced cementitious composites.

ACI member **Victor C. Li** is a Professor of Civil and Environmental Engineering at the University of Michigan. He is a member of ACI Committee 544, Fiber Reinforced Concrete. His research interests include micromechanics-based composite materials design and engineering, innovative structures design based on advanced materials technology, and sustainable infrastructure engineering.

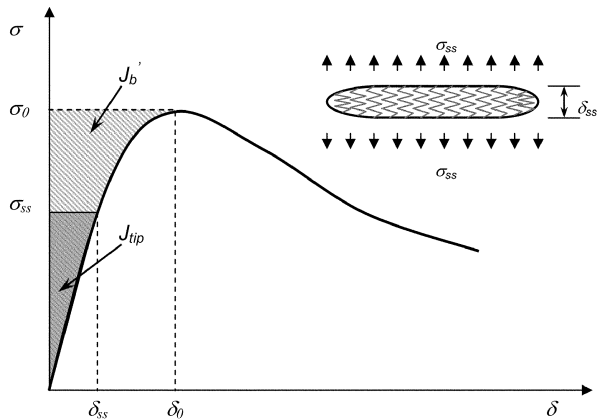


Fig. 1—Typical  $\sigma(\delta)$  curve for strain-hardening composite. Hatched area represents complementary energy  $J_b'$ . Shaded area represents crack tip toughness  $J_{tip}$ .

used mostly on construction-related applications,<sup>9</sup> while the remaining 75 million tons (165 million klb) were disposed by landfill. The use of CCPs offers environmental advantages by diverting the material from the waste stream, reducing the energy investment in processing virgin materials, conserving virgin materials, and allaying pollution. In this paper, the focus will be placed on the incorporation of fly ash and bottom ash into a PVA fiber reinforced ECC mixture. The high content of cement in a regular ECC mixture permits a high percentage of potential substitution by relatively low quality CCPs without significant compromise of strength development. In contrast, the emerging high performance, high volume fly ash (HVFA) concrete,<sup>10</sup> which may contain 50 to 60% fly ash by mass of total cementitious material, requires high-quality fly ash with low carbon content and high fineness to ease the adverse impact of high fly ash content on strength development, drying shrinkage, and durability that was often observed at high content substitution.<sup>11</sup>

Use of fly ash in fiber-reinforced cementitious composites has been investigated by a number of researchers in various systems.<sup>12,13</sup> However, little study has been carried out at the micromechanical level in conjunction with material tailoring for strain-hardening behavior. Nevertheless, it was observed that a high content of fly ash tends to reduce the bond strength and, in turn, facilitate fiber pullout.<sup>13</sup> In this paper, the influences of fly ash on the fiber matrix interface bond strength and matrix fracture toughness are quantitatively investigated in the context of designing composite for tensile strain hardening. Tensile behavior and strength development of ECC mixtures containing a high volume of fly ash and bottom ash are then examined. These findings highlight the feasibility of developing ECC materials with less environmental impact.

### RESEARCH SIGNIFICANCE

Material sustainability is rarely a concern in the development of current state-of-the-art HPRCC. High cement content is

commonly seen in the mixture design of these materials. This study demonstrates the feasibility of creating greener ECCs, which maintain the tensile ductility characteristics but also incorporate sustainability consideration. Effects of high volume recycled coal ash on the critical micromechanics parameters governing composite ductility were systematically investigated and effectively used to guide the mixture design. Such a micromechanics-based approach is also applicable to other material design practice. The development of greener ECCs will promote infrastructure sustainability through simultaneous enhancements of infrastructure durability and material greenness.

### ECC DESIGN GUIDELINE

The cornerstone of the theoretical framework of ECC development lies in the criteria of steady state crack propagation necessary for strain-hardening behavior. Early works by Marshall and Cox<sup>14</sup> on continuous fiber composites and later by Li and Leung<sup>15</sup> on discontinuous fiber composites translated the criteria into requirements on the fiber bridging properties, that is, bridging stress versus crack opening relation  $\sigma(\delta)$  with constrain of crack tip fracture toughness  $J_{tip}$ . As illustrated in Fig. 1, the steady state crack stress  $\sigma_{ss}$  must satisfy

$$\sigma_{ss} \delta_{ss} - \int_0^{\delta_{ss}} \sigma(\delta) d\delta = J_{tip} \quad (1)$$

where  $J_{tip}$  can be approximated by  $K_m^2/E_m$ ,  $K_m$  is the fracture toughness, and  $E_m$  is the matrix elastic modulus. The condition that steady state cracks can occur then can be expressed as

$$J_{tip} \leq \sigma_0 \delta_0 - \int_0^{\delta_0} \sigma(\delta) d\delta \equiv J_b' \quad (2)$$

where  $\delta_0$  is the crack opening corresponding to maximum bridging stress  $\sigma_0$ . The terms on the right hand side of the inequality sign in Eq. (2) are defined as complementary energy of the  $\sigma(\delta)$  relation (refer to Fig. 1 for interpretation of the terms in Eq. (1) and (2)).

Equation (2) is the fundamental criterion governing ECC design, which ensures the occurrence of multiple-cracking. The micromechanics study in ECC development involves two additional aspects: the influence of fiber and interface properties on the bridging behavior  $\sigma(\delta)$ , and the condition of developing saturated multiple cracking that links the composite ductility to both matrix toughness and flaw size distribution. The latter may become critical when limited margin between steady state cracking stress and peak fiber bridging stress prevails. In normal ECC materials without deliberate control of pre-existing flaw size distribution, the ratio  $J_b'/J_{tip}$  can be viewed as the multiple-cracking potential indicator.<sup>16</sup>

The effect of interface properties on  $J_b'$  is of great interest in the development of green ECCs due to the sensitivity of interface bond to the change of matrix composition. In this study, hydrophilic PVA fiber is used as the reinforcing fiber. PVA fiber possesses strong chemical affinity for cement hydration products, which has to be overcome before fiber can be pulled out. This debonding process can be modeled as a tunneling crack with characterizing interface fracture

energy, that is, chemical bond  $G_d$ . After debonding, the interface is considered to be dominated by a constant frictional stress  $\tau_0$ . During pullout, PVA fiber features extraordinary slip-hardening response,<sup>17</sup> and the coefficient  $\beta$  was introduced to describe the slip-hardening behavior.<sup>18</sup> Besides the interfacial properties, the  $\sigma(\delta)$  curve is also governed by the fiber content  $V_f$ , fiber diameter  $d_f$ , length  $L_f$ , and Young's Modulus  $E_f$ . Because this study focuses on matrix substitution, only one type of fiber is used and fiber volume fraction is fixed at 2.0%.

To illustrate the influence of fiber and interface parameters on fiber bridging behavior, Eq. (3) shows  $\sigma(\delta)$  relation for a special case where short fibers are aligned to tensile direction and no fiber rupture is considered. Slip-hardening is also neglected for simplicity.

$$\sigma(\delta) = \begin{cases} 2V_f \sqrt{(2G_d + \tau_0 \delta) \frac{E_f}{d_f}} - \frac{V_f E_f \delta}{L_f} & \delta \leq \delta_c \\ \frac{4V_f \tau_0 (L_f - \delta)^2}{L_f d_f} & \delta < \delta < \frac{L_f}{2} \end{cases} \quad (3)$$

where  $\delta_c$  is the crack opening when all fibers, regardless of the embedment length, finish debonding. An extended model of  $\sigma(\delta)$  accounting for random orientation of fibers, fiber rupture, slip-hardening, two-way pullout, and matrix spalling can be found in Reference 19. Complementary energy  $J_b'$  can be then be calculated as

$$J_b' = \frac{V_f \tau_0^2 L_f}{6d_f^2 E_f} - \frac{2V_f G_d L_f}{d_f} + \frac{8V_f G_d}{3\tau_0} \sqrt{\frac{2E_f G_d}{d_f}} - \frac{2V_f E_f G_d^2}{\tau_0^2 L_f} \quad (4)$$

Equation (4) can be further simplified by dropping the last two terms with relatively small values, so that

$$J_b' = V_f \frac{L_f}{d_f} \left( \frac{\tau_0^2 L_f^2}{6d_f E_f} - 2G_d \right) \quad (5)$$

Equation (5) indicates that high chemical bond  $G_d$  diminishes  $J_b'$  and reduces the multiple-cracking potential. Although Eq. (5) suggests that high interface friction  $\tau_0$  helps to improve  $J_b'$ , excessive  $\tau_0$  may cause fiber rupture during debonding and hence decrease  $J_b'$ . In fact, for PVA fiber, it was found that the interface friction exceeds the optimal value in typical mortar matrixes and needs to be reduced.<sup>2</sup> Therefore, a low chemical bond  $G_d$  and a moderate interface friction  $\tau_0$  is targeted in ECC material design.

The present study emphasizes the influence of fly ash substitution content on interface properties and therefore on the composite properties. It is speculated that the chemical bond of PVA fiber to surrounding matrix is tied to the concentration of reactive cement species while interface traction stress is governed by the microstructure of interfacial transition zone, for example, packing density and stiffness. Therefore, low reactivity ashes, such as ASTM C 618 Class F fly ash and even bottom ash that is usually considered unsuitable for use in portland cement concrete, are actually preferred to lower the strength of the interfacial chemical bond. These low reactivity ashes are mostly disposed to

**Table 2—ECC mixture proportions for micromechanics parameter study**

Mixture ID	Cement	Aggregates	Fly ash	Water	$w/cm^*$	HRWRA <sup>†</sup>	Fiber <sup>‡</sup>
	c	A/c	FA/c	w/c			
M41	1.0	0.8	0.1	0.27	0.24	0.03	0.02
M42	1.0	0.8	0.2	0.29	0.24	0.03	0.02
M43	1.0	0.8	0.8	0.43	0.24	0.03	0.02
M44	1.0	0.8	1.0	0.48	0.24	0.03	0.02
M45	1.0	0.8	1.2	0.53	0.24	0.03	0.02
M46	1.0	0.8	1.5	0.60	0.24	0.03	0.02

\*Water-to-cementitious material (cement + fly ash) ratio.

<sup>†</sup>Melamine formaldehyde sulfonate-based high-range water-reducing admixture.

<sup>‡</sup>PVA fiber is by volume fraction, and all others are by weight parts.

landfills due to lack of recycling value. On the other hand, control of interface properties can also be implemented through fiber surface treatment. A detailed study regarding the effect of oiling of PVA fiber surface on strain-hardening behavior can be found in Reference 2, and the optimized fiber is used in this study.

Besides interface tailoring, equally important to successful ECC design is the matrix toughness control, as implied by Eq. (2). The  $J_{tip}$  value has to be limited to below  $J_b'$ . In practice, some approaches can be used to lower  $J_{tip}$ , including an increase of the water-to-binder ratio (for example, regular PVA-ECC mixture<sup>2</sup>), use of inert filler, and exclusion of large aggregates. The last approach often results in high cement content. In the design of green ECCs, this can be counteracted by using high volume of low reactivity ashes, replacing a portion of the cement. Other types of powder from wastes can also be used, provided that fiber dispersion (for example, mixture rheology) is not affected adversely. The use of fly ash is expected to lead to a favorable reduction of the matrix toughness  $J_{tip}$ , which is examined in this paper.

The use of recycled waste material in ECCs may impair certain material performances, for example, compression strength. In particular, the lack or absence of quality control of the waste material could impart large variation to composite behavior. Therefore, it is emphasized in the ECC design that mixture proportion should be determined by material performances critical for the targeted application. Because brittleness is identified as one of the major bottlenecks in improving structure durability and serviceability, the focus of this study is placed on the tensile ductility. Material greenness is pursued while retaining high strain capacity.

## EXPERIMENTAL PROGRAM

The experimental program involves two sets of investigation. First, the influence of fly ash content on the micromechanics parameters including fiber/matrix interface properties and matrix toughness were quantified and correlated to composite tensile ductility. Second, the effect of various types of ashes on the composite behavior, in particular tensile behavior, was evaluated for high ash content mixture.

### Microscale investigation

Table 2 lists a set of mixture proportions used for micro-mechanics parameter study, where fly ash-to-cement ratio ranges from 0.1 to 1.5, while water-to-cementitious material ratio ( $w/cm$ ) is fixed at 0.24 to maintain similar fresh mixture consistency across all mixtures. ASTM Type I portland cement and a low-calcium Class F fly ash is used. Table 3 lists the chemical and physical properties of Class F fly ash.

**Table 3—Chemical and physical properties of Class F fly ash**

SiO <sub>2</sub> , %	54.08	Moisture content, %	0.81
Al <sub>2</sub> O <sub>3</sub> , %	23.40	Loss on ignition, %	1.00
Fe <sub>2</sub> O <sub>3</sub> , %	4.30	Amount retained on No. 325 sieve, %	25.57
Sum, %	81.78	Specific gravity	2.25
CaO, %	11.49	Autoclave soundness, %	-0.04
MgO, %	1.99	Strength activity index with portland cement at 7 days, percent of control	75.30
SO <sub>3</sub> , %	0.69		
Na <sub>2</sub> O, %	0.33	Strength activity index with portland cement at 28 days, percent of control	79.88
K <sub>2</sub> O, %	0.78		
Total alkalis, %	0.84	Water required, percent of control	90.90
Available alkalis, %	0.27		

**Table 4—Mixture proportions containing fly ash and other ashes**

Mixture ID	Cement, kg/m <sup>3</sup> (lb/yd <sup>3</sup> )	Aggregates, kg/m <sup>3</sup> (lb/yd <sup>3</sup> )	Ash, kg/m <sup>3</sup> (lb/yd <sup>3</sup> )	Water, kg/m <sup>3</sup> (lb/yd <sup>3</sup> )	HPMC, kg/m <sup>3</sup> (lb/yd <sup>3</sup> )	HRWRA, kg/m <sup>3</sup> (lb/yd <sup>3</sup> )	Fiber, kg/m <sup>3</sup> (lb/yd <sup>3</sup> )
ECC R0	838 (1412)	838 (1412)	—	366 (617)	1.26 (2.12)	17 (29)	26 (44)
ECC G0	583 (983)	467 (787)	700 (1180) (Bottom ash)	298 (502)	—	19 (32)	26 (44)
ECC G1	318 (536)	701 (1182)	509 (858) (Class F) 191 (322) (Fine fly ash)	289 (487)	0.16 (0.27)	19 (32)	26 (44)
ECC G2	318 (536)	701 (1182)	701 (1182) (Class F)	289 (487)	0.16 (0.27)	19 (32)	26 (44)
ECC G3	318 (536)	701 (1182)	191 (322) (Fine fly ash) 250 (421) (Class F) 250 (421) (Bottom ash)	289 (487)	0.16 (0.27)	19 (32)	26 (44)
ECC G4	318 (536)	701 (1182)	701 (1182) (Bottom ash)	289 (487)	0.24 (0.40)	19 (32)	26 (44)

Because large aggregates are excluded in ECC mixture design, only fine sand is incorporated. The silica sand used has a maximum 250 μm (0.01 in.) grain size and 110 μm (0.004 in.) average grain size. For composite tests, PVA fiber with a surface oil coating of 1.2% by weight was used throughout this study with a fixed volume fraction at 2%. The fiber had a diameter of 39 μm (0.0015 in.), a length of 12 mm (0.47 in.), and overall Young’s modulus of 25.8 GPa (3742 ksi). The apparent fiber strength is 1092 MPa (158 ksi).

**Composite investigation**

For the study on the influence of various types of ashes on the composite tensile behavior, a second series of ECC mixtures were employed. Table 4 includes mixture proportions of five ECC mixtures (ECC G0 to ECC G4) with high ash content, along with the reference regular PVA-ECC mixture (ECC R0) that does not contain fly ash. ECC G0 has the same proportion as M45, except that Class F fly ash is replaced by bottom ash. Low cement content is pursued in ECC G1 to ECC G4 by increasing the sand-to-cement ratio and ash-to-cement ratio to 2.5 each, and the variable investigated in these similar mixtures is the effect of various types of ashes and their combinations. Fine fly ash is a finely graded fly ash, and its particle size distribution (average 2 μm) is well below that of normal Class F fly ash (average 13 μm

**Table 5—Chemical and physical properties of fine fly ash**

SiO <sub>2</sub> , %	54.12	Moisture content, %	0.13
Al <sub>2</sub> O <sub>3</sub> , %	27.89	Loss on ignition, %	0.64
Fe <sub>2</sub> O <sub>3</sub> , %	4.77	Amount retained on No. 325 sieve, %	0.60
Sum, %	86.78	Specific gravity	2.51
CaO, %	6.72	Autoclave soundness, %	-0.06
MgO, %	1.66	Strength activity index with portland cement at 7 days, percent of control	108.8
SO <sub>3</sub> , %	0.80		
Na <sub>2</sub> O, %	0.44	Strength activity index with portland cement at 28 days, percent of control	121.9
K <sub>2</sub> O, %	1.17		
Total alkalis, %	1.21	Water required, percent of control	89.3
Available alkalis, %	N/A		

[0.0005 in.]) and bottom ash (average 50 μm [0.002 in.]). The chemical and physical properties of fine fly ash can be found in Table 5. The commercial value of fine fly ash is higher than Class F fly ash and much higher than bottom ash. This difference in the recycle value of these ashes motivates the study of the impact of various ash types on the ECC composite behavior, that is, the mixture design is considered increasingly environmental friendly from ECC G1 to G4. Viscosity agent hydroxypropyl methylcellulose (HPMC) and high-range water-reducing admixture (HRWRA) were both found necessary in high-volume ash ECC mixtures for achieving adequate workability.

**Specimen preparation and testing**

All mixtures were prepared in a mixer with a 10 L (2.65 gal.) capacity. The solid ingredients, including cement, sand and fly ash, and HPMC powder if applicable were first mixed for approximately 1 minute, and then water was added and mixed for another 3 minutes before HRWRA was added into the mixer. Once a consistent mixture was reached, fiber was added. The finished fresh mixture showed good flowability and could be easily cast into molds without applying vibration. Specimens were demolded after 24 hours and then cured in water at room temperature 16 to 20 °C (61 to 68 °F) before testing. At least three specimens were tested for each case.

Fiber/matrix interfacial properties were measured by a single fiber pullout test, where a single fiber with a controlled embedment length is pulled out from a block of matrix and the load-versus-displacement relation was recorded. Details of specimen preparation and test method can be found in Reference 2. Data interpretation and calculation of the interface parameters including frictional stress τ<sub>0</sub>, chemical bond G<sub>d</sub>, and slip-hardening coefficient β follow Reference 17.

Matrix fracture energy J<sub>tip</sub> was determined by a wedge splitting test<sup>20</sup> in which the vertical load applied on the wedge and crack opening at the loading position were recorded. The ECC block specimen measured 100 x 100 x 100 mm (4 x 4 x 4 in.) and the uncracked ligament length was 50 mm (2 in.). Matrix fracture toughness K<sub>m</sub> was measured by three-point bending test compliant to ASTM E 399. The beam specimen of the matrix mixture without fiber measured 304.8 mm (12 in.) in length by 76.2 mm (3 in.) in height by 38.1 mm (1.5 in.) in depth, and the loading support spanned 254.0 mm (10 in.). The notch depth to height ratio was 0.4.

All compressive tests use 75 mm (3 in.) in diameter by 150 mm (6 in.) in height cylinder specimens. The ends of the specimens were capped with sulfur compound. Testing began at 3 hours after casting or when adequate strength had

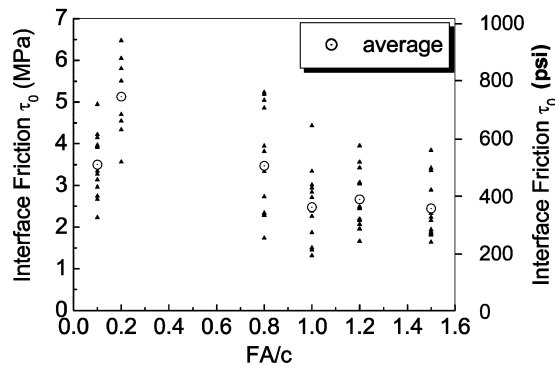


Fig. 2—Decrease of interface friction at high fly ash content.

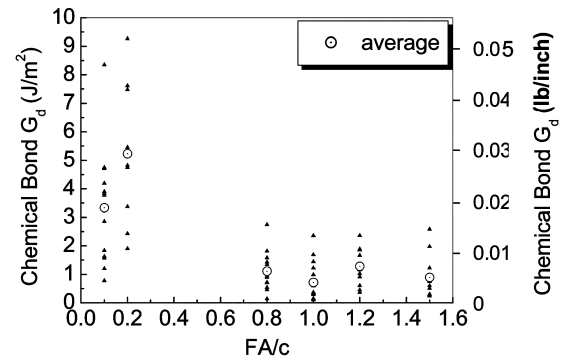


Fig. 3—Low chemical bond of PVA fiber to matrix at high fly ash content.

developed. The age of the specimen was recorded as the time elapse from finish of casting to test. The mixing and casting procedure took approximately 20 to 30 minutes.

Direct uniaxial tensile test was conducted to characterize the tensile behavior of the ECC material.<sup>2</sup> The coupon specimen used herein measures 304.8 x 76.2 x 12.7 mm (12 x 3 x 0.5 in.). Aluminum plates were glued at the ends of the coupon specimen to facilitate gripping. Tests were conducted under displacement control at a loading rate of 0.005 mm/second (0.0002 in./second). Two external linear variable displacement transducers were attached to the specimen surface with a gauge length of approximately 180 mm (7.1 in.) to measure the displacement.

## EXPERIMENTAL RESULTS

### Microscale study

Fiber/matrix interface parameters determined from a single fiber pullout test (Mixtures M41 to M46) are summarized in Fig. 2 through 4. The specimens were tested at an age of 3 months. Despite large data variation, as is typical of this type of test, a general descending trend with an increase of fly ash content was observed for both frictional stress and chemical bond except for FA/c = 0.1 (M41), while chemical bond showed a more significant drop at high ash content. The  $G_d$  value for M46 of 0.90 J/m<sup>2</sup> (0.005 lb/in.) is considered rather low for PVA fiber.<sup>2</sup> In contrast, the slip-hardening coefficient exhibits little dependence on fly ash content. The data scattering was caused by the hydrophilic nature of the PVA fiber and the resulting small embedment length necessary for fiber to be pulled out.

Typical wedge splitting test results of M41 to M46 mixtures are shown in Fig. 5, where the area under the splitting force-versus-displacement relation can be interpreted as fracture energy. Because only fine sand is used in the matrixes, the brittleness is apparent. Quick load drop occurs after peak load, and the ascending branch shows little nonlinearity. With increase of fly ash content, crack initiation stress decreases significantly, which is desirable to improve strain-hardening potential as discussed earlier. Figure 6(a) summarizes the matrix fracture energy  $J_{tip}$  determined from a wedge-splitting test, showing considerable dependence of  $J_{tip}$  on fly ash content. The descending trend seems to flatten after FA/c = 1.2. At FA/c = 1.2 and 1.5,  $J_{tip}$  decreases to 16 J/m<sup>2</sup> (0.09 lb/in.), approximately half of that at FA/c = 0.1. Figure 6(b) shows matrix fracture toughness  $K_m$  measured from a three-point bending test, and a similar trend is observed. The tensile properties of composite M41 to M46 obtained from a uniaxial tension test, including first cracking strength, ultimate strength, and corresponding strain, are listed in Table 6. The

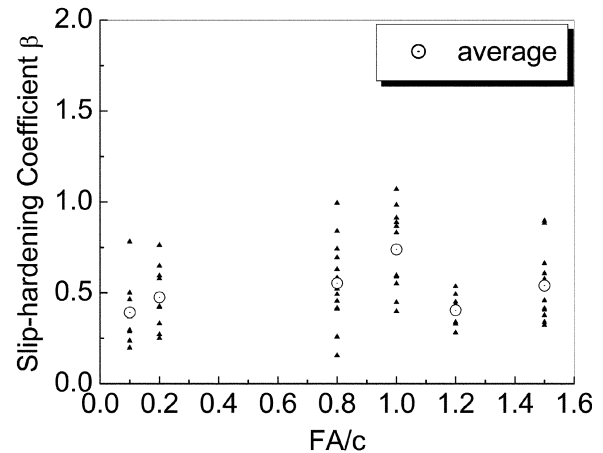


Fig. 4—Independence of interface slip-hardening coefficient on fly ash content.

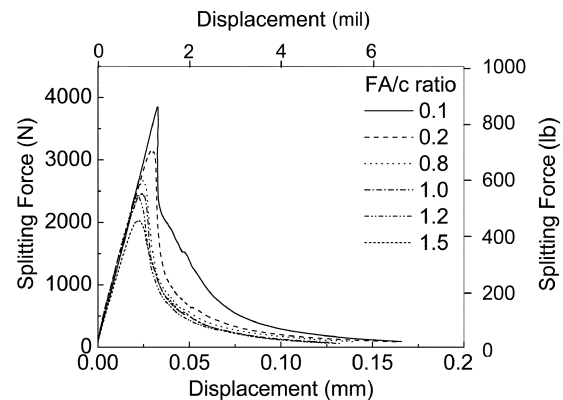


Fig. 5—Wedge splitting force versus displacement relationships at different fly ash-to-cement ratios (note: 1 mil = 0.001 in.).

specimen age at test is 3 months. Clear multiple cracking pattern emerges at FA/c = 0.8 and above. With the exception of M43, first cracking strength and ultimate strength slightly decrease with an increase of fly ash content. Because first cracking strength is governed by matrix fracture toughness and largest flaw size oriented to the loading direction, lower matrix toughness at high ash volume will certainly lead to lower cracking strength, provided flaw size distribution inherent from processing details is similar in all mixtures. Inspection of the protruded fibers at the failure surface revealed significant fiber rupture in all mixtures, but average

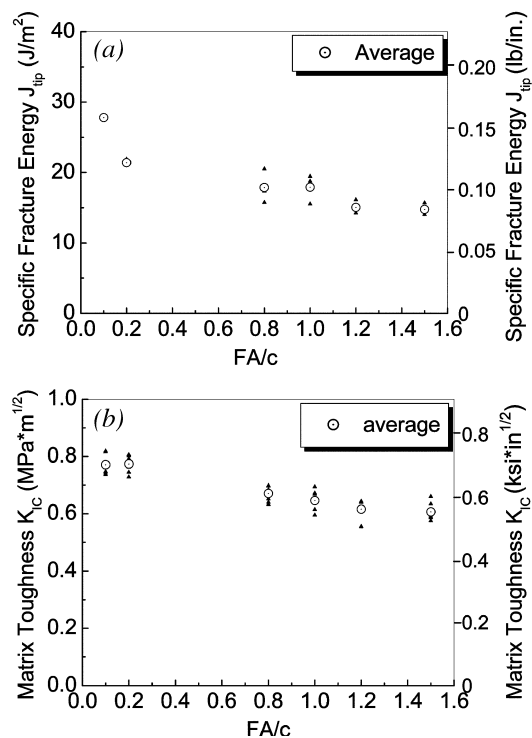


Fig. 6—Descending trend of  $J_{tip}$  and  $K_m$  with increase of fly ash content: (a) specific fracture energy  $J_{tip}$  from wedge splitting test; and (b) matrix (without fibers) fracture toughness determined from three-point bending test.

Table 6—Tensile properties of ECC mixtures

Mixture ID	First-cracking strength, MPa (psi)	Ultimate tensile strength, MPa (psi)	Tensile strain capacity, %
M41	4.64 ± 0.47 (672.8 ± 68.15)	5.48 ± 0.24 (794.6 ± 34.8)	0.37 ± 0.07
M42	4.58 ± 0.06 (664.1 ± 8.7)	5.60 ± 0.09 (812 ± 13.05)	0.66 ± 0.17
M43	3.95 ± 0.10 (572.75 ± 14.5)	4.72 ± 0.53 (684.4 ± 76.85)	1.11 ± 0.51
M44	4.42 ± 0.27 (640.9 ± 39.15)	5.56 ± 0.26 (806.2 ± 37.7)	1.98 ± 0.62
M45	4.11 ± 0.66 (595.95 ± 95.7)	4.86 ± 0.47 (704.7 ± 68.15)	2.49 ± 0.57
M46	3.69 ± 0.44 (535.05 ± 63.8)	4.47 ± 0.26 (648.15 ± 37.7)	2.69 ± 0.37
ECC R0	2.92 ± 0.06 (423.4 ± 8.7)	4.41 ± 0.15 (639.45 ± 21.75)	4.88 ± 0.59
ECC G0	3.30 ± 0.10 (478.5 ± 14.5)	4.14 ± 0.07 (600.3 ± 10.15)	3.41 ± 0.69
ECC G1	3.80 ± 0.15 (551 ± 21.75)	4.23 ± 0.22 (613.35 ± 31.9)	1.54 ± 1.33
ECC G2	3.69 ± 0.22 (535.05 ± 31.9)	4.80 ± 0.25 (696 ± 36.25)	3.90 ± 0.61
ECC G3	3.92 ± 0.12 (568.4 ± 17.4)	4.77 ± 0.54 (691.65 ± 78.3)	4.29 ± 0.57
ECC G4	3.08 ± 0.05 (446.6 ± 7.25)	4.35 ± 0.16 (630.75 ± 23.2)	3.95 ± 0.17

protruded length increases at high ash content, indicating the percentage of fiber rupture in fact declines for those high ash content mixtures. Because more fibers are pulled out instead of rupture, the maximum bridging stress that fibers can reach will decrease consequently. The strain capacity, however, shows steady improvement and stabilizes at 2.5% at FA/c = 1.2 and 1.5 (Table 6).

## Composite performance

Test Set M41 to M46 reveals an unambiguous weakening effect of fly ash on both interfacial bond and matrix toughness, both of which are desirable in ECC design. Adequate interface and matrix parameters were reached at FA/c = 1.2 and above. Based on these findings, mixture proportions of greener ECCs, that is, ECC G0 to ECC G4, were designed. Figure 7 shows the tensile stress versus strain relations of these mixtures, along with that of the reference ECC R0 without fly ash. The tensile properties are also summarized in Table 6. Except for ECC G0, which was tested at an age of 3 months, other mixtures presented in Fig. 7 were tested at the age of 28 days.

Significant strain hardening and saturated multiple cracking were generally observed in ECC mixtures with high volume fly ash. Robust tensile strain capacity between 3 to 4% was demonstrated except for ECC G1. The performance of ECC G2 and G3 surpass the reference ECC R0 containing high volume cement in terms of strength. Replacement of Class F fly ash with bottom ash, for example, M45 versus G0 and G2 versus G4, leads to noticeable reduction in first-cracking strength due to the inert nature of bottom ash. In contrast, high ash content in ECC G1 to ECC G3 has little influence on the composite first-cracking strength compared with M46. However, partial replacement with fine fly ash shows little advantage on improving the tensile behavior. Indeed, the higher reactivity of the fine fly ash is expected to lead to a higher matrix toughness and interfacial chemical bond strength in ECC G1, in comparison with M45, which has the same total amount of fly ash, so that a lower tensile strain capacity of ECC G1 results. In ECC G3, the higher reactivity of the fine fly ash is balanced out by the lower reactivity of the bottom ash.

Figure 8 shows the development of steady state crack opening in ECC G2 with increasing strain. The crack width is controlled under 80  $\mu$ m (0.0032 in.). In contrast to conventional fiber reinforced concrete with tension-softening behavior, the maximum crack width of ECCs before failure is bounded by the crack opening corresponding to peak fiber bridging strength, and is innately a property of the material (independent of steel reinforcement ratio or structural size<sup>21</sup>).

The compressive strength development of these ECC mixtures up to 8 months are summarized in Fig. 9. Because G1 to G4 have similar cement content to normal structural concrete, it is not surprising that they exhibit similar strength gain rate. The compressive strength at 3 days is approximately 12 MPa (1740 psi), which is considered sufficient for framework removal. At 28 days, compressive strength of G2 and G3 exceeds 35 MPa (5075 psi). The ash type, however, shows significant effect on strength development. Mixture ECC G4 with bottom ash gained strength slower than G2 with Class F fly ash, and ECC G1 outpaced similar mixtures with the advantage of reactive fine ash.

## DISCUSSION

The weakening effect of ash on interface parameters may arise from two separate mechanisms, that is, change of matrix chemical composition and coating effect of inert particles on fiber surface. The chemical bond of PVA fiber to cementitious matrix is believed to be governed by the metal cation concentration at the interface, in particular Al<sup>3+</sup> and Ca<sup>2+</sup>. In the study of macro-defect-free cement, for example, PVA polymer-bound calcium aluminate cement (C<sub>3</sub>A), it was found that Al<sup>3+</sup> and Ca<sup>2+</sup> are responsible for the formation of a strong interphase thin layer between

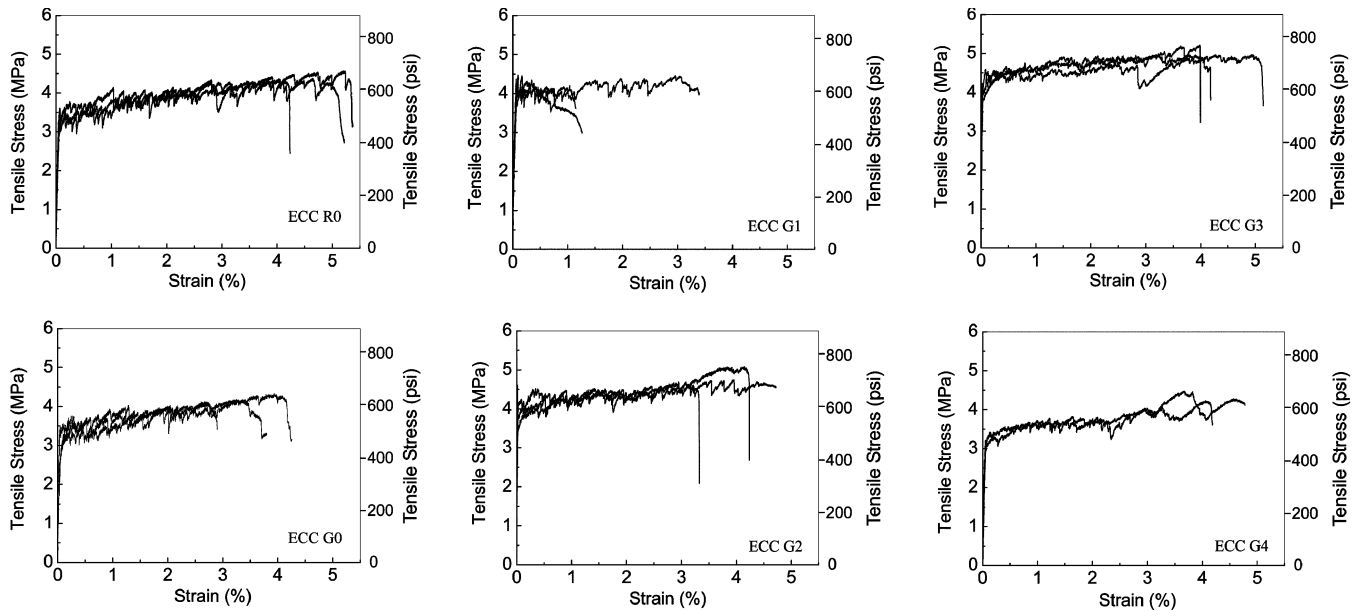


Fig. 7—Tensile behavior of ECC mixtures with high ash content.

cement grain and PVA bulk polymer.<sup>22,23</sup> In ordinary portland cement,  $Al^{3+}$  exists in the forms of  $C_3A$  and  $C_4AF$  in small amounts, and most of them react with gypsum to form insoluble sulfo-aluminate hydrates. In fact, buildup of  $Ca(OH)_2$  crystals at the PVA fiber surface was observed.<sup>24</sup> In fly ash, most  $Al^{3+}$  and  $Ca^{2+}$  are not free. Hence, high volume fraction of low calcium Class F fly ash dilutes the concentration of  $Al^{3+}$  and  $Ca^{2+}$  in matrix and reduces the possibility of developing a strong chemical bond. In contrast, frictional bond is closely related to the packing density and stiffness of the interfacial transition zone. Therefore, chemical bond is more sensitive to the ash content than the frictional stress, which is evident from the data in Fig. 2 and 3. In addition, the average  $G_d$  measured at high FA/c is generally lower than that of ECC R0 ( $1.6 J/m^2$  [0.009 lb/in.], refer to Reference 2), which does not contain fly ash though the matrix is less compact due to a high  $w/cm$  of 0.45. Mixtures M41 to M46 all have low  $w/cm$  ( $= 0.24$ ). Frictional stress in these mixtures (2.5 to 5.1 MPa [363 to 740 psi]), however, is significantly higher than that of ECC R0 (1.1 MPa [160 psi]).

The second mechanism contributing to interface property change involves aggregation of inert particles on PVA fiber surface, in particular, amorphous carbon. Residual carbon from insufficient combustion exists in almost all types of ashes and is the main component responsible for the loss of ignition (LOI). The carbon content in ashes varies significantly from source to source, but typically Class F fly ash has higher carbon content than Class C fly ash. The particular Class F fly ash used in this study, however, has a low carbon content of 1%, while the bottom ash contains significant amounts of residual carbon. It was noticed that the PVA fiber washed out from fresh ECC mixtures with high volumes of Class F fly ash had a light gray color and fibers washed out from mixtures with bottom ash had a black color, in contrast to the original light yellow color. The color of washed-out fibers would not change if the mixture does not contain ash. Figure 10(a) shows the picture of PVA fiber washed out from mixture containing bottom ash, and aggregation of sub-micron particles on the fiber surface can clearly be seen. XEDS analysis indicated that carbon element concentration

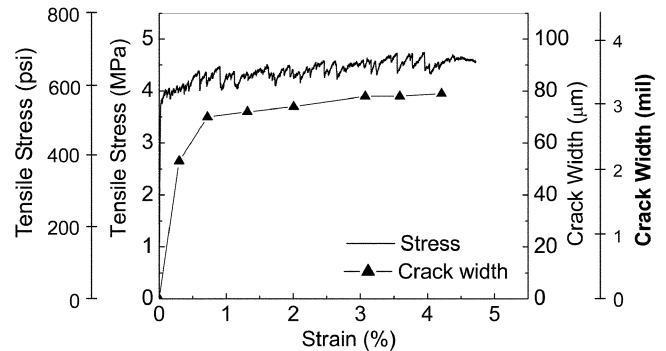


Fig. 8—Controlled crack opening of green ECC G2 (note: 1 mil = 0.001 in.).

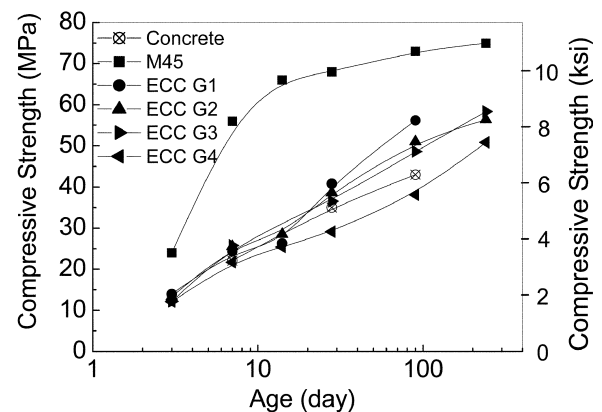


Fig. 9—Comparison of 8-month compressive strength development of green ECC mixtures with normal concrete.

at the surface of these washed-out fibers is significantly higher than that of virgin fibers. Figure 10(b) shows the surface of PVA fiber pulled out from composite matrix, and no particles coating is observed. The evidence supports that carbon particles tend to concentrate on the PVA fiber surface during mixing, providing extra lubricant for fiber pullout in

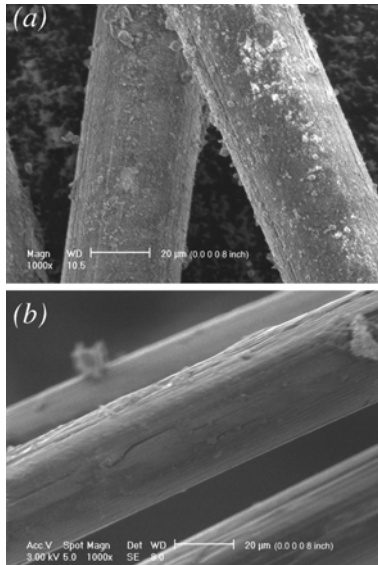


Fig. 10—PVA fiber surface morphology of washed-out fiber and pulled-out fiber: (a) washed-out PVA fiber from fresh mixture with bottom ash; and (b) pulled-out PVA fiber from composite.

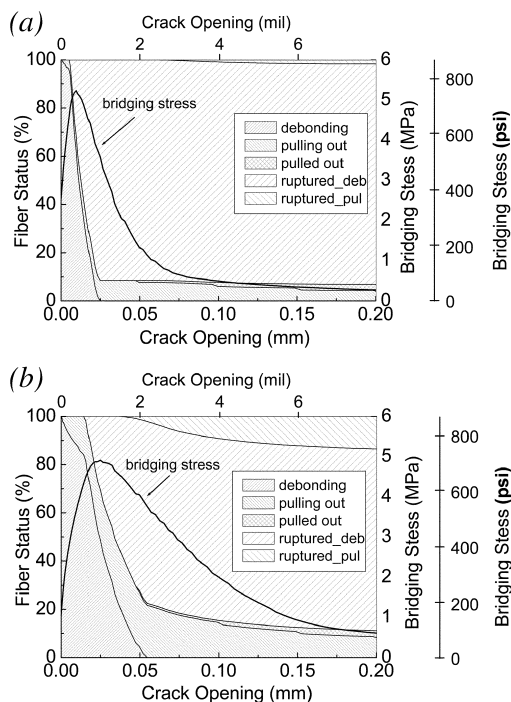


Fig. 11—Fiber status and bridging stress versus crack opening relation of: (a) M42; and (b) M46, showing significant delay of fiber rupture in M46. Each area represents one of five statuses that fiber belongs: debonding, pulling out, pulled out, ruptured during debonding, and ruptured during pullout. Matrix spalling is not accounted in calculating crack opening.

addition to the oil coating. Mechanically, the presence of carbon coating reduces frictional stress, and may also weaken the chemical bond. This is particularly evident in mixtures with bottom ash, where larger crack width and crack spacing were observed. Therefore, carbon content in ash could be an influential factor pertaining to ECC performance.

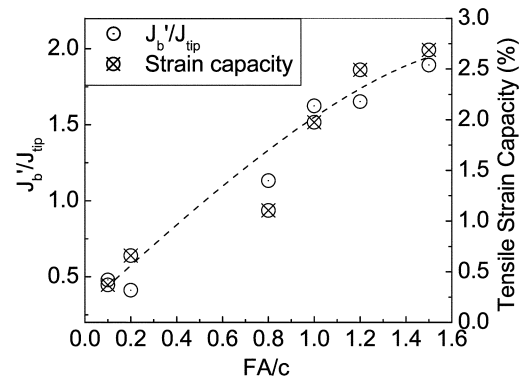


Fig. 12—Correlation between  $J_b'/J_{tip}$  and tensile strain capacity.

Reduction of interface bond in the presence of high ash content leads to less fiber rupture. For a fiber with one end embedded in the matrix, the maximum embedment length that allows fiber to complete debonding without rupture can be calculated as

$$L_c = \frac{\sigma_f d_f - \sqrt{8G_d E_f (1 + \eta) d_f}}{4\tau_0 (1 + \eta)} \quad (6)$$

where  $\sigma_f$  is the fiber strength. Obviously, any decrease in either chemical bond  $G_d$  or frictional stress  $\tau_0$  allows more fibers to enter pullout stage, which is critical for increasing  $J_b'$  and hence improving strain-hardening potential. Figure 11 illustrates evolution of fiber status in composites M42 and M46 with an increase of the crack opening (represented by hatched areas). The corresponding  $\sigma(\delta)$  relation is also shown on the plot. The comparison clearly reveals the significant delay of fiber rupture in M46 at the same crack opening due to lower interfacial bond parameters. For instance, at a crack opening of 25  $\mu\text{m}$  (0.001 in.), 9% of the fibers in M42 were in pullout stage and the rest ruptured during debonding, while in M46, only 32% fibers ruptured and the percentage of fibers in debonding and pullout stages were 48 and 20%, respectively. Fiber bridging behavior as well as the complementary energy  $J_b'$  thereafter alters significantly. It should be mentioned that the theoretical model adopted in this paper does not account for the relaxation effect of matrix spalling and, as a result, the crack opening corresponding to the peak bridging stress is more or less underestimated. The conclusion drawn herein, however, should not be affected.

For ECC mixtures with inherent flaw size distribution, the ratio of  $J_b'$  to  $J_{tip}$  is often used as an indicator of multiple cracking potential. Figure 12 shows  $J_b'/J_{tip}$  ratio and strain capacity in the same plot against fly ash content. The strong correlation between these two parameters is evident. It should be mentioned that relaxation due to matrix spalling at fiber exit to crack surface is not accounted in the computation of  $J_b'$  herein, therefore, the theoretical value is underestimated. Strictly speaking, multiple cracking can only occur when  $J_b'/J_{tip} > 1$ . Nevertheless, the plot shows that significant multiple cracking emerges at  $J_b'/J_{tip} > 1$ , which is corresponding to  $FA/c = 0.8$ , and strain capacity continues to increase with  $J_b'/J_{tip}$  at the same pace, supporting that  $J_b'/J_{tip}$  can be treated as a robust indicator for strain capacity.

## CONCLUSIONS

High volume coal combustion by-products including fly ash and bottom ash were incorporated into ECC mixtures with the intention of improving their sustainability performance. Micromechanics tools were used to guide the design process for maximizing strain-hardening potential. The resulting composites demonstrated robust tensile strain capacity at 3 to 4% and tensile strength above 4.5 MPa (653 psi) while material sustainability indexes were significantly improved.

The micromechanics parameter study revealed the general descending trend of interface frictional stress and chemical bond with increase of fly ash content, which in turn modifies the PVA fiber-bridging behavior resulting in higher  $J_b'$  values. In addition, an increase of fly ash content also leads to a lowering of the matrix toughness  $J_{tip}$ . Both trends are favorable to strain hardening. Strong correlation between  $J_b'/J_{tip}$  and strain capacity was observed, which further support this ratio as a good indicator of composite strain-hardening potential.

It is shown that a proper mixture designing process can achieve high material performance even when using low-quality waste products as cement substitutions, as long as the governing micromechanics parameters were carefully controlled. Although this study focused on tensile ductility of cementitious composites, the authors believe that this approach is broadly applicable to other sustainable material design practice.

## ACKNOWLEDGMENTS

This research was funded through an NSF MUSES Biocomplexity Program Grant (CMS-0223971 and CMS-0329416). MUSES (Materials Use: Science, Engineering, and Society) supports projects that study reducing adverse human impact on the total interactive system of resource use, the design and synthesis of new materials with environmentally benign impacts on biocomplex systems, as well as maximizing the efficient use of individual materials throughout their life cycles. Partial support from the Knud Hojgaard Foundation at the Technical University of Denmark is also gratefully acknowledged. The authors would like to thank G. Keoleian at the School of Natural Resource and Environment, University of Michigan, for assistance in materials sustainability assessment; H. Stang and L. Østergaard at the Technical University of Denmark for assistance in conducting the wedge splitting test; and E. H. Yang in the preparation of the final version of this manuscript.

## REFERENCES

1. Li, V. C., "Engineered Cementitious Composites—Tailored Composites Through Micromechanical Modeling," *Fiber Reinforced Concrete: Present and the Future*, N. Banthia, A. A. Bentur, and A. Mufti, eds., Canadian Society for Civil Engineering, Montreal, Quebec, Canada, 1998, pp. 64-97.
2. Li, V. C.; Wu, C.; Wang, S.; Ogawa, A.; and Saito, T., "Interface Tailoring for Strain-Hardening Polyvinyl Alcohol-Engineered Cementitious Composite (PVA-ECC)," *ACI Materials Journal*, V. 99, No. 5, Sept.-Oct. 2002, pp. 463-472.
3. Li, V. C., "Strategies for High Performance Fiber Reinforced Cementitious Composites Development," *Fiber Reinforced Concrete: From Theory to Practice*, Proceedings of the North American/European Workshop on Advances in Fiber Reinforced Concrete, S. Ahmad, M. di Prisco, C. Meyer, G. A. Plizzari, and S. Shah, eds., Bergamo, Italy, 2004, pp. 93-98.
4. Li, V. C., "From Micromechanics to Structural Engineering—The Design of Cementitious Composites for Civil Engineering Applications," *Journal of Structural Mechanics and Earthquake Engineering*, JSCE, V. 10, No. 2, 1993, pp. 37-48.
5. Li, V. C., "Reflections on the Research and Development of Engineered Cementitious Composites (ECC)," *Proceedings of the JCI International Workshop on Ductile Fiber Reinforced Cementitious Composites (DFRCC)—Application and Evaluation*, Takayama, Japan, Oct. 2002, pp. 1-21.
6. Battelle, "Climate Change," *Toward a Sustainable Cement Industry*, World Business Council on Sustainable Development (WBCSD), Mar. 2002, 92 pp.
7. Lankard, D. R., and Newell, J. K., "Preparation of Highly Reinforced Steel Fiber Reinforced Concrete Composites," *Fiber-Reinforced Concrete—International Symposium*, SP-81, G. C. Hoff, ed., American Concrete Institute, Farmington Hills, Mich., 1984, pp. 286-306.
8. VSL, "Introduction to Ductal—Frequently Asked Questions," May 2005, <http://www.ductal.com>, 17 pp.
9. American Coal Ash Association, "2003 Coal Combustion Product (CCP) Production and Use Survey," Oct. 2004.
10. Mehta, P. K., "Reducing the Environmental Impact of Concrete," *Concrete International*, V. 23, No. 10, Oct. 2001, pp. 61-66.
11. Mehta, P. K., "Greening of the Concrete Industry for Sustainable Development," *Concrete International*, V. 24, No. 7, July 2002, pp. 23-28.
12. Guerrero, P., and Naaman, A. E., "Effect of Mortar Fineness and Adhesive Agents on Pullout Response of Steel Fibers," *ACI Materials Journal*, V. 97, No. 1, Jan.-Feb. 2000, pp. 12-20.
13. Peled, A.; Cyr, M. F.; and Shah, S. P., "High Content of Fly Ash (Class F) in Extruded Cementitious Composites," *ACI Materials Journal*, V. 97, No. 5, Sept.-Oct. 2000, pp. 509-517.
14. Marshall, D. B., and Cox, B. N., "A J-Integral Method for Calculating Steady-State Matrix Cracking Stresses in Composites," *Mechanics of Materials*, No. 8, 1988, pp. 127-133.
15. Li, V. C., and Leung, C. K. Y., "Theory of Steady State and Multiple Cracking of Random Discontinuous Fiber Reinforced Brittle Matrix Composites," *Journal of Engineering Mechanics*, ASCE, V. 118, No. 11, 1992, pp. 2246-2264.
16. Kanda, T., and Li, V. C., "A New Micromechanics Design Theory for Pseudo Strain Hardening Cementitious Composite," *Journal of Engineering Mechanics*, ASCE, V. 125, No. 4, 1999, pp. 373-381.
17. Redon, C.; Li, V. C.; Wu, C.; Hoshiro, H.; Saito, T.; and Ogawa, A., "Measuring and Modifying Interface Properties of PVA Fibers in ECC Matrix," *Journal of Materials in Civil Engineering*, ASCE, V. 13, No. 6, 2001, pp. 399-406.
18. Wang, Y.; Li, V. C.; and Backer, S., "Modeling of Fiber Pull-Out from a Cement Matrix," *International Journal of Cement Composite Lightweight Concrete*, V. 10, No. 3, 1988, pp. 143-149.
19. Wang, S., "Micromechanics Based Matrix Design for Engineered Cementitious Composites," PhD thesis, University of Michigan, Ann Arbor, Mich., Apr. 2005, 222 pp.
20. Østergaard, L., "Early-Age Fracture Mechanics and Cracking of Concrete: Experiments and Modeling," PhD Thesis, Technical University of Denmark, Lyngby, Denmark, 2003, 263 pp.
21. Li, V. C., and Stang, H., "Elevating FRC Material Ductility to Infrastructure Durability," *Fiber-Reinforced Concretes*, M. di Prisco, R. Felicetti, and G. A. Plizzari, eds., 2004, pp. 171-186.
22. Rodger, S. A.; Brooks, S. A.; Sinclair, W.; Groves, G. W.; and Double, D. D., "High Strength Cement Pastes," *Journal of Materials Science*, V. 20, 1985, pp. 2853-2860.
23. Gulgun, M. A.; Kriven, W. M.; Tan, L. S.; and McHugh, A. J., "Evolution of Mechano-Chemistry and Microstructure of a Calcium Aluminate-Polymer Composite: Part I—Mixing Time Effects," *Journal of Materials Research*, V. 10, No. 7, July 1995, pp. 1746-1755.
24. Chan, Y. W., "Fiber/Cement Bond Property Modification in Relation to Interfacial Microstructure," PhD thesis, University of Michigan, Ann Arbor, Mich., July 1994, 173 pp.